RSC Advances

PAPER

View Article Online
View Journal | View Issue

Cite this: *RSC Adv.*, 2018, **8**, 13018

Positively charged and flexible SiO_2@ZrO_2 nanofibrous membranes and their application in adsorption and separation†

Yufei Tang, Zhaowei Liu, Kang Zhao * and Song Fu

Tiny particles with a negative charge in water can be removed effectively by inorganic positively charged nanofiber membranes due to their physical separation and electrostatic adsorption properties. However, the charged positive and isoelectric points (IEP) on the surface of the positively charged nanofiber membranes need to be further improved to meet the requirements of the Environmental Protection Agency for virus filters (excellent adsorption and separation properties in solutions with pH between 5 and 9). The positively charged SiO_2@ZrO_2 nanofibrous membrane was fabricated by electrospinning combined with the impregnation method and calcined in an anoxic atmosphere. The effects of the impregnating solution concentration and centrifugal speeds on the morphology, pore size and nanofiber diameter of the composite nanofibrous membrane were investigated. The phase composition, the element valence state, the surface charge and the adsorption separation properties of the composite nanofibrous membranes were characterized. Flexible SiO_2@ZrO_2 nanofibrous membranes with high specific surface area and water flux were obtained. The surface isoelectric point is 7.3 when calcined in a mixed atmosphere of N_2 (96%)/H_2 (4%), which is higher than that when calcined in air and vacuum. Some oxygen vacancies were present on the surface of the ZrO_x ($0 < x < 2$) shell, resulting in the tetragonal zirconia still being available at room temperature. The interception rate of the positively charged SiO_2@ZrO_2 nanofibrous membranes for a titan yellow solution with a concentration of 10 mg L^{-1} reaches 99.996%. Its maximum adsorption capacity can reach 63.27 mg cm^{-3} when filtering a 1 L titan yellow solution. The resulting nanofibrous membranes have potential application for the separation of bacteria and viruses from water.

Received 4th March 2018
Accepted 2nd April 2018

DOI: 10.1039/c8ra01899e

rsc.li/rsc-advances

Introduction

Adsorption and separation materials are widely used in sewage purification, mineral water removal of bacteria and gas purification.[1,2] Porous ceramic materials have attracted much attention in the field of filtration and separation because of their excellent properties such as chemical stability, high temperature resistance, and corrosion resistance.[3,4] Generally, the objects removed to achieve the goal of purification by porous ceramic materials were removed based on the ceramic porous structure, mainly through physical adsorption and interception.[5,6] Therefore, the open porosity and specific surface area of porous ceramic materials are important factors that can affect the filtration efficiency.[7,8] Many methods have been used to prepare porous ceramic materials with high open porosity and high specific surface area, such as dip-molding and freeze casting.[9–11] The porous ceramics obtained by these methods can remove impurities of a large size only. However, for some small size particles, such as dyes (<100 nm), bacteria (<1 μm) and viruses (<100 nm), adsorption and interception properties have been found to be poor mainly because of the large size of the pores (>2 μm) of porous ceramics.[12–14]

Electrospinning is a method of preparing nanofibers using a high voltage electrostatic field.[15,16] The spinnable polymer and the ceramic precursor were mixed to prepare a spinning solution, and then porous ceramic fibrous membranes were obtained after calcination.[17,18] The pore size of the porous fibrous membranes was usually not greater than 1 μm, the electrospun material does not form closed pores, and a high specific surface area can be obtained.[19,20] Porous fibrous membranes can be used as the separation material through their physical sieving effect of the pores. Smaller pore size corresponds to better filtration and separation performance. However, the water flux is low when the pore size is too low, and the liquid requires high pressure to pass through the membrane. The stability of the ceramic fibrous membrane will also be reduced due to its brittleness. If the surface of the porous fibrous membranes is positively charged, negative particles would be adsorbed and

Department of Materials Science and Engineering, Xi'an University of Technology, Xi'an 710048, PR China. E-mail: kzhao@xaut.edu.cn; Fax: +86-29-82312922; Tel: +86-29-82312922

† Electronic supplementary information (ESI) available. See DOI: 10.1039/c8ra01899e

removed by electrostatic adsorption.[21,22] It is possible to adsorb small size bacteria (<1 μm) and viruses (<100 nm) with negative charged surface using large pore size (100 nm to 2 μm) materials with positive charged (above the isoelectric point in solutions). In previous work, we have used the electrostatic spinning to fabricate the ZrO_2 nanofibrous microfiltration membrane.[23] The isoelectric point is only 4.3, and the separation range of the ZrO_2 nanofibrous microfiltration membrane was narrow. The isoelectric point of the ZrO_2 nanofiber can be increased by calcining in the vacuum but only up to 4.7. In the vacuum calcination, the decomposition of the spinnable polymer is incomplete, giving rise to the presence of residual carbon in the ZrO_2 nanofiber, and this also reduces the mechanical properties of the microfiltration membrane.

To solve these problems, we attempt to prepare SiO_2 nanofiber membranes by electrospinning and then obtain the SiO_2@ZrO_2 nanofibrous membranes following impregnation. This approach will not produce a residual carbon in an oxygen-lacking atmosphere and was beneficial for increasing the positive charge on the membrane surface because the ZrO_2 shell was impregnated without polymer additives. The obtained membranes also showed flexibility due to the characteristics of amorphous SiO_2. Effects of the impregnating solution content and the centrifugal speed on the morphologies, pore size and nanofiber diameter of SiO_2@ZrO_2 nanofibrous membranes were investigated and their phase composition, elemental valence state and the positive charge were characterized. Adsorption and separation properties of SiO_2@ZrO_2 nanofibrous membranes for titan yellow (simulating the negative charge of a virus) at different environmental conditions were also tested. The obtained membranes show prospects for broad applications in the fields of infectious virus protection, water treatment, pharmaceutical production and biological engineering.

Experimental

Materials and methods

Tetraethoxysilane (TEOS, AR, Tianjin Kermel Chemical Reagent Co., Ltd., Tianjin, China) and zirconium oxychloride (AR, Tianjin Guangfu Fine Chemical Research Institute, Tianjin, China) were used as Si and Zr precursors, respectively. Ethanol (AR, Anhui Ante Biochemical Co., Ltd., Suzhou, Anhui, China), *N*′*N*-dimethylformamide (AR, Tianjin Kermel Chemical Reagent Co., Ltd., Tianjin, China) and deionized water were used as solvents. Phosphoric acid (AR, Tianjin Yaohua chemical reagents Co., Ltd., Tianjin, China) was used as a hydrolysant for TEOS. Polyvinyl alcohol (PVA, M_w = 60 000) and polyvinylpyrrolidone (PVP, M_w = 1 300 000) were purchased from Sigma Aldrich and used as spinnable polymers.

PVA was added to the deionized water at 70 °C to obtain the PVA solution by stirring for 6 h. TEOS was added to the deionized water and then the SiO_2 solution was obtained by adding the phosphoric acid to hydrolyze the TEOS. The SiO_2 solution was slowly added into the PVA solution to obtain the SiO_2 spinning solution. The SiO_2 spinning solution was loaded into a micropump, and PVA/SiO_2 composite nanofibers were obtained after electrospinning. Spinning parameters were as follows: spinning voltage of 20 kV, receiving distance of 15 cm, propulsion rate of 0.4 mL h^{-1}, ambient temperature of 40 °C and relative humidity of 40%. Then, the PVA/SiO_2 composite nanofibers were calcined for 2 h at 600 °C to obtain the SiO_2 nanofibrous membranes. The impregnated solution was obtained by mixing $ZrOCl_2$ in deionized water. SiO_2 nanofibrous membranes were impregnated for 2 h and were centrifuged for 3 min to dry. Finally, coaxial SiO_2@ZrO_2 nanofibrous membranes were obtained by calcination at 700 °C in vacuum or in 4% H_2/96% N_2 mixed atmosphere for 2 h.

Characterization

Morphologies of SiO_2@ZrO_2 nanofibrous membranes were characterized by SEM (JSM 6700F, JEOL, Japan) and using a stereo microscope (OLYMPUS, Tokyo, Japan). The pore size of the membranes and the diameter of the SiO_2@ZrO_2 coaxial nanofibers were determined by Smile View (Software, JEOL, Japan) using SEM images; here, 50 pores and 50 nanofibers were tested in this manner to obtain the distribution and the average value. X-Ray diffraction (XRD; Model 7000, Shimadzu Corporation, Tokyo, Japan) was used to identify the phases in the membranes. The core/shell structure and the components of the SiO_2@ZrO_2 nanofibers were characterized by TEM (JEM-3010, JEOL, Japan). The specific surface areas of the nanofibrous membranes were characterized using a model BK122T-B analyzer by N_2 adsorption at −196 °C. The mechanical property of the nanofibrous membranes was tested with a fibers strength tester (LLY-06E, YuanMore, Shaoxing, China). The nanofibrous membranes were cut into rectangular pieces sized length × width = 10 mm × 4 mm (the thickness was about 0.6 mm). Tensile rate was 10 mm min^{-1}. The zeta potential of SiO_2@ZrO_2 nanofibers was determined using a microelectrophoresis instrument (JS94H, Shanghai zhongchen digital technology equipment Co. Ltd., China). Chemical compositions and binding energy of Zr 3d were analyzed by X-ray photoelectron spectroscopy (XPS, AXIS-ULTRA DLD, Shimadzu Corporation, Tokyo, Japan). Water flux was determined by a membrane flux meter (MF/UF, Hydra Netherlands); test parameters: effective filtration area of 12.56 cm^2, thickness of 1 mm, operation pressure of 1 Pa. The adsorption and separation properties of the positively charged SiO_2@ZrO_2 nanofibrous membranes were characterized using titan yellow (with 2 negative charges) as the simulated virus. The standard absorbance curve was obtained using a UV-visible spectrophotometer (UV-5100, METASH, China) using titan yellow solutions with different concentrations. The titan yellow solution (10 mg L^{-1}) with different pH values was filtered using the SiO_2@ZrO_2 nanofibrous membranes. The absorbance of the original solution and that the filtered solution were determined, and the interception rate was calculated using eqn (1).

$$R = \left(1 - \frac{A_1}{A_2}\right) \times 100\% \quad (1)$$

where R is the interception rate, A_1 is the absorbance of the original titan yellow solution, and A_2 is the absorbance of the

filtered titan yellow solution. A 1 L titan yellow solution (10 mg L^{-1}) was filtered to determine the maximum adsorption capacity of the SiO_2@ZrO_2 nanofibrous membranes.

Results and discussion

Morphologies and composites of electrospun SiO_2@ZrO_2 nanofibrous membranes

Impregnation was found to be an effective method for the preparation of coaxial nanofibers.[24] $ZrOCl_2$ contents of the impregnating solutions had an important influence on the morphology of the nanofibrous membranes. Fig. 1 shows the morphologies of SiO_2@ZrO_2 nanofibrous membranes obtained by impregnating solutions with different contents. The centrifugal speed was 5000 rpm. The coaxial nanofiber after impregnation was still a long continuous nanofiber with a smooth surface. When the $ZrOCl_2$ content of the impregnated solution increases to 3 mol L^{-1}, some adhesion occurred between the coaxial nanofibers. Some connections between the nanofibers were observed when the $ZrOCl_2$ content reaches 4 mol L^{-1}. The impregnated solution was easily aggregated at the junction of the nanofibers due to the surface tension effect when the $ZrOCl_2$ content increases, and it was difficult to remove it from the centrifuge, and the joint is formed at the lap of nanofibers after drying and sintering. However, this connection does not have a negative impact on the morphologies of the SiO_2@ZrO_2 nanofibrous membranes in addition to a slight impact on the surface area. ZrOCl was adsorbed on the surface of SiO_2 when impregnating, and the ZrO_2 shell can finally be formed in the oxygen-lacking atmosphere.

Pore size distributions of the SiO_2@ZrO_2 nanofibrous membranes and diameters distribution of the SiO_2@ZrO_2 nanofibers were characterized, as shown in Fig. 2. With the increase of the $ZrOCl_2$ contents of the impregnated solutions, the average pore size of the SiO_2@ZrO_2 nanofibrous membranes decreased from 756.2 nm to 721.2 nm, but the main distribution range of the pore size did not change, which is closely related to the diameter of the SiO_2@ZrO_2 nanofibers. The

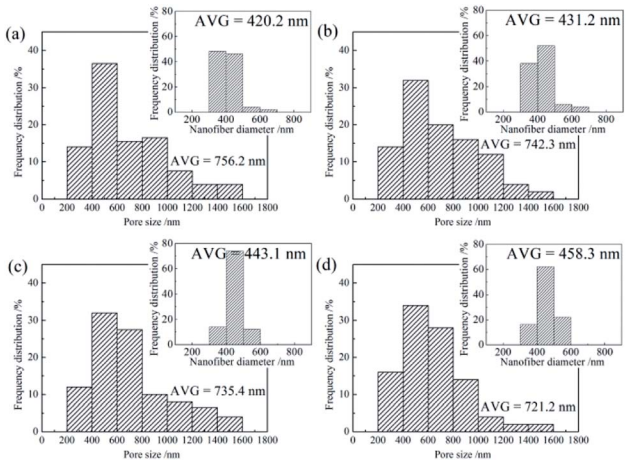

Fig. 2 Pore size distributions of SiO_2@ZrO_2 nanofibrous membranes obtained by impregnating solutions with different $ZrOCl_2$ contents: (a) 1; (b) 2; (c) 3; (d) 4 mol L^{-1}.

average diameter of the SiO_2@ZrO_2 nanofibers increased from 420.2 nm to 458.3 nm with the increase of the $ZrOCl_2$ content, and the number of the nanofibers between 300 and 400 nm decreased significantly (images in insets of Fig. 2). This is mainly because the increase in the $ZrOCl_2$ content can increase the thickness of the ZrO_2 shell. The increase of the SiO_2@ZrO_2 nanofibers diameter leads to the decrease of the pore size of the nanofibrous membranes.

Fig. 3 shows the macro morphology of the SiO_2@ZrO_2 nanofibrous membranes. The SiO_2@ZrO_2 nanofibrous membrane shows excellent flexibility and can bend to form a O shape with the diameter of 10 mm. This flexibility is mainly due to the character of the SiO_2 core. The SiO_2 core of the coaxial nanofibers is amorphous and is mainly connected by an infinite SiO_4 tetrahedral network. Since the size of the core is very small, the volume percentage of the SiO_2 internal boundary increases, which means that more atoms can be assigned to the boundary.[25,26] Therefore, a large reduction in the stress concentration reduces the extension of micro-cracks on the SiO_2 nanofiber. Although the shell consists of brittle ZrO_2, the

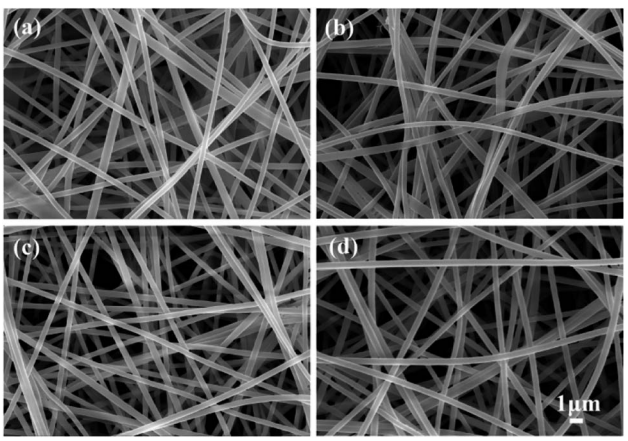

Fig. 1 Morphologies of SiO_2@ZrO_2 nanofibrous membranes obtained by impregnating solutions with different $ZrOCl_2$ contents: (a) 1; (b) 2; (c) 3; (d) 4 mol L^{-1}.

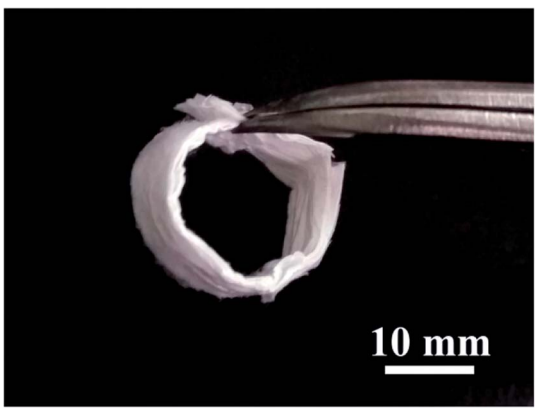

Fig. 3 Macro morphology of flexible SiO_2@ZrO_2 nanofibrous membranes.

SiO_2@ZrO_2 nanofiber shows flexibility because of its small thickness, which is beneficial to the stability of filtration.

Fig. 4 shows the XRD patterns of the SiO_2@ZrO_2 nanofibrous membranes. The diffraction peak of SiO_2 was not found because the SiO_2 obtained by electrospinning usually was amorphous. Strong diffraction peaks of the membranes coincided with the characteristic peaks of the ($\bar{1}$11), (111) and (220) planes in the monoclinic ZrO_2 (JCPDS 37-1484). Some weak diffraction peaks coincided with the (101), (002) and (200) characteristic peaks in the tetragonal ZrO_2 (JCPDS 42-1164). The ZrO_2 shell of the coaxial nanofibers was mainly found in the monoclinic phase and contains a small amount of tetragonal phase.

The microstructure and composition of SiO_2@ZrO_2 nanofibrous membranes were further characterized by XPS, as shown in Fig. 5. Fig. 5(a) shows the TEM micrograph of the SiO_2@ZrO_2 nanofiber. The obvious coaxial structure was observed. The black part was the core of the coaxial nanofiber, which is a SiO_2 nanofiber obtained by electrospinning. The light gray region was the ZrO_2 shell of the coaxial nanofiber, with the thickness of approximately 10–30 nm. In the HRTEM micrograph of the SiO_2@ZrO_2 nanofiber (Fig. 5(b)), the dark region was amorphous and was speculated to be amorphous SiO_2. The interplanar spacing of the light-colored shell was 0.316 nm, corresponding to the ($\bar{1}$11) plane of monoclinic-ZrO_2 and indicating that the ZrO_2 shell was mainly found in the monoclinic phase. The ZrO_2 shell was further amplified, as shown in Fig. 5(c). It can be observed that the grain size of ZrO_2 was about 15 nm.

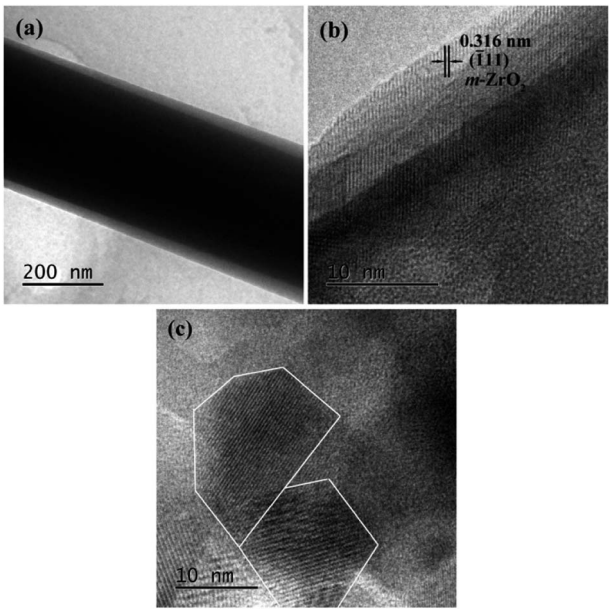

Fig. 5 (a) TEM micrograph of the SiO_2@ZrO_2 nanofiber; (b) HRTEM micrograph of the SiO_2@ZrO_2 nanofiber; (c) magnification of (b).

Specific surface area and water flux of SiO_2@ZrO_2 nanofibrous membranes

Fig. 6 shows the water fluxes and specific surface areas of SiO_2@ZrO_2 nanofibrous membranes with different average pore sizes. With the increase of the pore size of the SiO_2@ZrO_2 nanofibrous membranes, the water flux decreases, and the specific surface area decreases. When the average pore size was 768.2 nm, the maximum water flux was 643.1 L $(m^2\ h)^{-1}$ and the specific surface area was 265.1 $m^2\ g^{-1}$, which is mainly related to the diameter of SiO_2@ZrO_2 nanofibers. Together with the results presented in Fig. 1, this shows that the large pore size of the nanofibrous membranes was obtained by a small nanofiber diameter, which is beneficial for the solution flow through the membrane. Meanwhile, the specific surface area also reached the maximum value, which can improve the filtration efficiency and adsorption capacity of the SiO_2@ZrO_2 nanofibrous membranes.

In practical use, the positive charged SiO_2@ZrO_2 nanofibrous membranes should be mechanically strong enough to bear the water flux. The tensile strength of SiO_2@ZrO_2 nanofibrous membranes was tested and the stress–strain curve was shown in Fig. 7. With the increase of the applied tensile strain, the SiO_2@ZrO_2 nanofibrous membrane broke in a mild style. The tensile strength was 0.24 MPa, which was higher than that of the SiO_2 filtration film reported in the literature.[27]

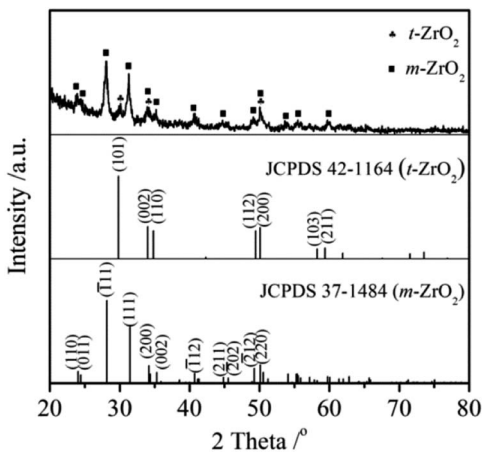

Fig. 4 XRD patterns of SiO_2@ZrO_2 nanofibrous membranes.

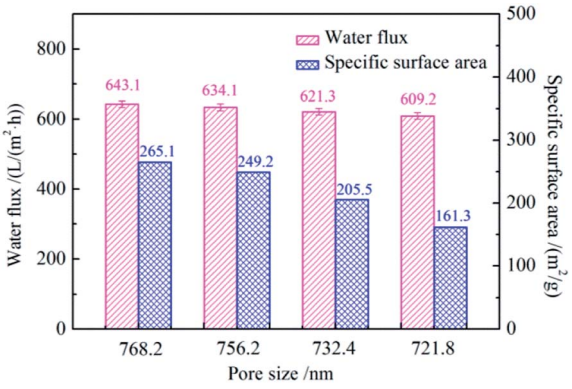

Fig. 6 Water fluxes and specific surface areas of SiO_2@ZrO_2 nanofibrous membranes with different average pore sizes.

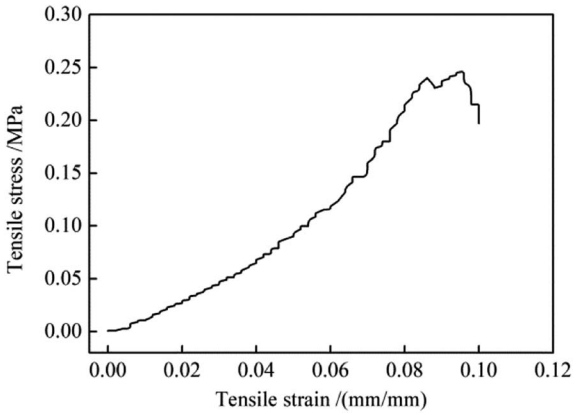

Fig. 7 Stress–strain curve of SiO_2@ZrO_2 nanofibrous membranes with the pore size of 768.2 nm.

Positive charged properties of SiO_2@ZrO_2 nanofibrous membranes

The SiO_2@ZrO_2 nanofibrous membrane with the largest water flux and specific surface area was selected for the testing of its surface zeta potential under different pH, and the results for the samples with the calcination performed in different atmospheres were compared, as shown in Fig. 8. The surface zeta potentials of SiO_2@ZrO_2 nanofibrous membranes calcined in air, vacuum and in 96% N_2/4% H_2 atmosphere decrease with increasing pH. Zeta potentials of the calcined nanofibrous membranes in the mixed atmosphere were slightly higher than that of the vacuum calcined nanofibrous membranes. The isoelectric point (IEP) of the SiO_2@ZrO_2 nanofibrous membranes after calcination at vacuum was 7.1, and the IEP was 7.4 after calcination of 96% N_2/4% H_2, which is much larger than and the IEP (4.5) of that calcined in air and also the IEP of ZrO_2 nanofiber membrane.[23] The IEP of the SiO_2@ZrO_2 nanofibrous membranes can be obviously increased by calcining in 96% N_2/4% H_2 mixture atmosphere, because the oxygen vacancy concentration of ZrO_2 surface can be increased, resulting in the IEP shifting to the right.

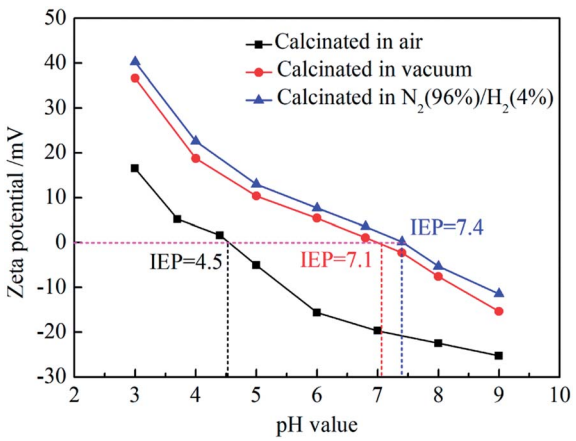

Fig. 8 Zeta potentials of surfaces on SiO_2@ZrO_2 nanofibrous membranes in solutions with different pH values.

To further analyze the ZrO_2 oxygen vacancies in the SiO_2@ZrO_2 nanofibrous membranes, XPS was used to perform elemental analysis and the peak fitting of the Zr element was carried out in detail, as shown in Fig. 9. Fig. 9(a) shows full spectrum of the positively charged SiO_2@ZrO_2 nanofibrous membranes calcinated in vacuum and in 96% N_2/4% H_2 mixture. The components of the SiO_2@ZrO_2 nanofibrous membranes were Zr, Si and O (C was the calibrated element). Fig. 9(b) shows the peak fitting curves of the Zr 3d fine spectrum. Electron binding energies of Zr 3d5/2 in the ZrO_2 shell of vacuum-calcined nanofibrous membranes were 182.8 and 180.9 eV (electron binding energies of 3d3/2 were 180.4 and 179.5 eV), corresponding to ZrO_2 and ZrO_x ($0 < x < 2$),[28,29] respectively. This indicates that the surface of the SiO_2@ZrO_2 nanofibrous membranes contains oxygen vacancies. The binding energy of Zr in the ZrO_2 shell of nanofibrous membranes after calcining in 96% N_2/4% H_2 mixture atmosphere still corresponded to ZrO_2 and ZrO_x ($0 < x < 2$), respectively. The increase of ZrO_x content indicates that the number of oxygen vacancies on the surface of the fiber increases after the calcining of the 96% N_2/4% H_2 mixture atmosphere. A higher oxygen vacancy content gives rise to the increased zeta positive potential of the SiO_2@ZrO_2 nanofibrous membrane and increases the positive charge on

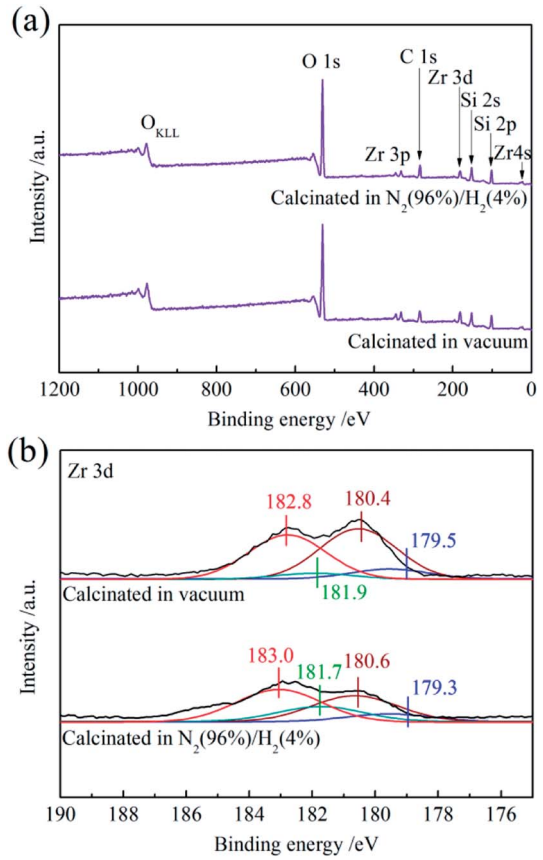

Fig. 9 XPS spectra of positively charged SiO_2@ZrO_2 nanofibrous membranes calcinated in vacuum and N_2 (96%)/H_2 (4%) mixture: (a) full spectrum and (b) Zr 3d.

the nanofiber surface. According to XRD analysis, ZrO_2 was mainly in the monoclinic phase, but some tetragonal phases were present as well, which may be related to the existence of oxygen vacancies. It is generally believed that the existence of the tetragonal phase in the oxygen-lacking conditions is due to the oxygen vacancies.[30] The surface of the sample may form a structure with an oxygen vacancy distortion, which can prevent the transformation from the monoclinic phase to the tetragonal phase.[31] Despite the exposure to air, the transformation of the tetragonal phase into the monoclinic phase still takes a long time due to the instability of the surface.

Adsorption and separation properties of positive charged SiO_2@ZrO_2 nanofibrous membranes

The separation of positively charged SiO_2@ZrO_2 nanofibrous membranes for electrical neutral materials was mainly due the physical sieving effect, and there is an electrostatic adsorption between the negatively charged material on the positively charged membrane.[32] The titan yellow with two negative charges was used to characterize the separation property of the positively charged SiO_2@ZrO_2 nanofibrous membranes. The charged fiber membrane was electrically neutral with no charge at the IEP. When the pH value was less than the IEP, titan yellow was separated by the adsorption on the positively charged nanofibrous membranes. Fig. 10 shows the interception rates of the positively charged SiO_2@ZrO_2 nanofibrous membranes for a titan yellow solution at different pH values. The interception rate of SiO_2@ZrO_2 nanofibrous membranes calcinated in air was 99.99% in titan yellow solution with pH = 3–3.5. The interception rate decreased rapidly at pH > 3.5, and was only 0.06% at pH = 9. The interception rate of the vacuum-calcined SiO_2@ZrO_2 nanofibrous membranes in the solution with pH value from 3 to 6.5 remains above 99.996%. The interception rate decreased rapidly when the pH value of the solution was greater than 6.5, because the positively charge of the surface decreases and the interception mechanism for titan yellow was physical only. The titan yellow can pass through SiO_2@ZrO_2 nanofibrous membranes under pressure, so that the interception rate was very low. The interception rate of 96% N_2/4% H_2 mixture atmosphere calcined nanofibrous membranes was consistent with that of the vacuum-calcined nanofibrous membranes. However, the interception rate for titan yellow was higher than that of the vacuum-calcined nanofibrous membranes for the pH value of the solution in the 6.5–7.5 range. The interception rate was closely related to the positive charge of the nanofiber surface. The greater the positive charge, the higher the interception rate for the pH value smaller than the IEP.

Fig. 11 shows the adsorption capacities of the positively charged SiO_2@ZrO_2 nanofibrous membranes for a titan yellow solution at different pH. Adsorption capacity of SiO_2@ZrO_2 nanofibrous membranes calcined in air were observed when the pH was lower than 4. When pH was higher than 6, the adsorption capacity was 0. The saturation adsorption capacity of the SiO_2@ZrO_2 nanofibrous membranes calcined in vacuum and N_2 (96%)/H_2 (4%) mixture at pH = 3–6.5 was reached, and the maximum saturated adsorption capacity was 64.36 mg cm^{-3}. When the pH was higher than 6.5, the saturation adsorption capacity rapidly decreases, and reaches the minimum value of only approximately 0.03 mg cm^{-3} for pH 8. Adsorption capacities of SiO_2@ZrO_2 nanofibrous membranes calcinated in the N_2 (96%)/H_2 (4%) mixture atmosphere and vacuum were basically the same. The SiO_2@ZrO_2 nanofibrous membranes surface has a strong positive charge in the solution with the pH lower than the IEP, so that the membrane can intercept the titan yellow molecules by electrostatic adsorption. When the pH of the solution was above the IEP, the saturated adsorption capacity of SiO_2@ZrO_2 nanofibrous membranes decreased rapidly due the absence of adsorption for the membrane surface with a negative charge. Nanofibrous membranes can only intercept a small amount of titan yellow by the mechanism of physical interception. Thus, higher pH corresponds to greater electronegativity and lower adsorption capacity.

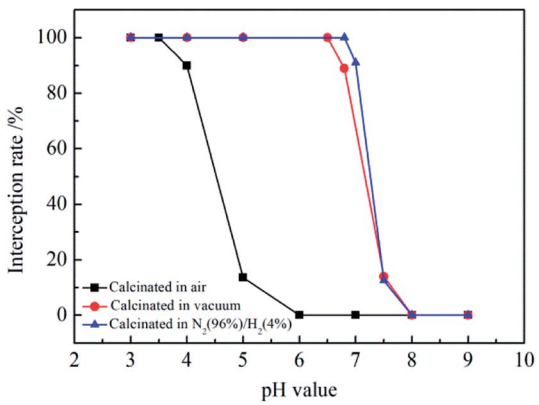

Fig. 10 Interception rates of positively charged SiO_2@ZrO_2 nanofibrous membranes calcined in air, vacuum and N_2 (96%)/H_2 (4%) mixture for titan yellow solution for different pH values.

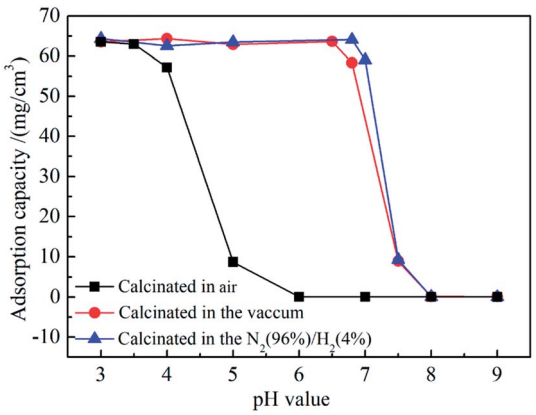

Fig. 11 Adsorption capacities of positively charged SiO_2@ZrO_2 nanofibrous membranes calcinated in air, vacuum and N_2 (96%)/H_2 (4%) mixture for titan yellow solution at different pH.

Conclusions

SiO_2@ZrO_2 coaxial nanofibrous membranes were prepared by electrospinning and impregnation in oxygen-lacking atmospheres. The resulting nanofibrous membranes show excellent flexibility. The maximum specific surface area of the SiO_2@ZrO_2 nanofibrous membrane with the pore size in 721.8–768.2 nm range can reach 249.24 m^2 g^{-1}, and the maximum water flux was 643.1 L $(m^2\ h)^{-1}$. SiO_2@ZrO_2 nanofibrous membranes obtained by calcining in oxygen-lack atmosphere consist of a monoclinic phase and a small amount of a tetragonal phase. Oxygen vacancies were found on their surface, and Zr is found in a low oxidation state. Calcining in the 96% N_2/4% H_2 mixture atmosphere can improve the IEP of the membrane to 7.3. The maximum water flux of SiO_2@ZrO_2 nanofibrous membranes was 643 L $(m^2\ h)^{-1}$ when the effective filtration area was 12.56 cm^2, the membrane thickness was 1 mm and the operating pressure was 1 Pa. Furthermore, the interception rate of the 96% N_2/4% H_2 mixture atmosphere calcined membrane for 20 mL titan yellow solution with the concentration of 10 mg L^{-1} reached 99.996% for the pH of less than 6.7. The saturated adsorption capacity reached 63.27 mg cm^{-3} for the filtration of 1 L titan yellow solution. The adsorption and separation of SiO_2@ZrO_2 nanofibrous membranes calcined in the 96% N_2/4% H_2 mixture atmosphere were greater than those in air and vacuum, which is mainly due to the increase of the surface oxygen vacancies and the positive surface charge. These positively charged SiO_2@ZrO_2 nanofibrous membranes utilize physical separation and electrostatic adsorption to effectively remove negatively charged particles; this outcome has potential application in the separation of bacteria and viruses from water. However, nanofibrous membranes with the excellent adsorption and separation properties in water with pH between 5 and 9 need to be obtained by increasing the IEP, meeting the requirements of the Environmental Protection Agency for virus filters. This is still the main direction of future experiments.

Conflicts of interest

There are no conflicts to declare.

Acknowledgements

The authors would like to acknowledge the support from the National Natural Science Foundation of China (No. 51572217), the China Postdoctoral Science Foundation (No. 2015M582689) and the Postdoctoral Science Foundation of Shaanxi Province (No. 2016BSHEDZZ03).

References

1 H. van der Laan, D. van Halem, P. W. M. H. Smeets, A. I. A. Soppe, J. Kroesbergen, G. Wubbels, J. Nederstigt, I. Gensburger and S. G. J. Heijman, Bacteria and virus removal effectiveness of ceramic pot filters with different silver applications in a long term experiment, *Water Res.*, 2014, **51**, 47–54.

2 N. Shirasaki, T. Matsushita, Y. Matsui, M. Kobuke and K. Ohno, Comparison of removal performance of two surrogates for pathogenic waterborne viruses, bacteriophage Qβ and MS2, in a coagulation–ceramic microfiltration system, *J. Membr. Sci.*, 2009, **326**, 564–571.

3 Y. Kamato and Y. Suzuki, Reactively sintered porous $MgAl_2O_4$, for water-purification filter with controlled particle morphology, *Ceram. Int.*, 2017, **43**, 14090–14095.

4 M. Sarro, N. P. Gule, E. Laurenti, R. Gamberini, M. C. Paganini, P. E. Mallon and P. Calza, Freeze casting of novel porous silicate cement supports using tert-butyl alcohol-water binary crystals as template: Microstructure, strength and permeability, *J. Membr. Sci.*, 2017, **541**, 143–152.

5 N. Kouras, A. Harabi, F. Bouzerara, L. Foughali, A. Policicchio, S. Stelitano, F. Galiano and A. Figoli, Macroporous ceramic supports for membranes prepared from quartz sand and calcite mixtures, *J. Eur. Ceram. Soc.*, 2017, **37**, 3159–3165.

6 Y. Lv, H. Liu, Z. Wang, S. Liu, L. Hao, Y. Sang, D. Liu, J. Wang and R. I. Boughton, Silver nanoparticle-decorated porous ceramic composite for water treatment, *J. Membr. Sci.*, 2009, **331**, 50–56.

7 S. Barg, D. Koch and G. Grathwohl, Processing and properties of graded ceramic filters, *J. Am. Ceram. Soc.*, 2009, **92**, 2854–2860.

8 J. Gröttrup, F. Schütt, D. Smazna, O. Lupan, R. Adelung and Y. K. Mishra, Porous ceramics based on hybrid inorganic tetrapodal networks for efficient photocatalysis and water purification, *Ceram. Int.*, 2017, **43**, 14915–14922.

9 C. R. Bowen and T. Thomas, Macro-porous Ti2AlC MAX-phase ceramics by the foam replication method, *Ceram. Int.*, 2015, **41**, 12178–12185.

10 S. Deville, E. Saiz and A. P. Tomsia, Ice-templated porous alumina structures, *Acta Mater.*, 2007, **55**, 1965–1974.

11 Y. Tang, S. Qiu, C. Wu, Q. Miao and K. Zhao, Freeze cast fabrication of porous ceramics using tert-butyl alcohol–water crystals as template, *J. Eur. Ceram. Soc.*, 2016, **36**, 1513–1518.

12 R. Sondhi, Y. S. Lin and F. Alvarez, Crossflow filtration of chromium hydroxide suspension by ceramic membranes: fouling and its minimization by backpulsing, *J. Membr. Sci.*, 2000, **174**, 111–122.

13 Y. Tang, M. Mao, S. Qiu and K. Zhao, Fabrication of porous ceramics with double-pore structure by stepwise freeze casting using water/diphenyl methane emulsion, *Ceram. Int.*, 2018, **44**, 1187–1192.

14 J. Maurath, J. Dittmann, N. Schultz and N. Willenbacher, Fabrication of highly porous glass filters using capillary suspension processing, *Sep. Purif. Technol.*, 2015, **149**, 470–478.

15 H. Fong and D. H. Reneker, Electrospinning and formation of nanofibers in *Structure formation in polymeric fibers*, ed. D. R. Salem, Hanser Publishers, Munich, 2001, pp. 225–246.

16 M. Bognitzki, W. Czado, T. Frese, A. Schaper, M. Hellwig, M. Steinhart, A. Greiner and J. H. Wendorff, Nanostructured fibers *via* electrospinning, *Adv. Mater.*, 2001, **13**, 70–72.

17 M. Sarro, N. P. Gule, E. Laurenti, R. Gamberini, M. C. Paganini, P. E. Mallon and P. Calza, ZnO-based materials and enzymes hybrid systems as highly efficient catalysts for recalcitrant pollutants abatement, *Chem. Eng. J.*, 2018, **334**, 2530–2538.

18 S. Zhan, D. Chen, X. Jiao and Y. Song, Mesoporous TiO_2/SiO_2 composite nanofibers with selective photocatalytic properties, *Chem. Commun.*, 2007, **20**, 2043–2045.

19 R. Allabashi, M. Arkas, G. Hörmann and D. Tsiourvas, Removal of some organic pollutants in water employing ceramic membranes impregnated with cross-linked silylated dendritic and cyclodextrin polymers, *Water Res.*, 2007, **41**, 476–486.

20 S. Abbasizadeh, A. R. Keshtkar and M. A. Mousavian, Preparation of a novel electrospun polyvinyl alcohol/titanium oxide nanofiber adsorbent modified with mercapto groups for uranium(VI) and thorium(IV) removal from aqueous solution, *Chem. Eng. J.*, 2013, **220**, 161–171.

21 B. L. T. Lau, G. W. Harrington, M. A. Anderson and I. Tejedor, Removal of nano and microparticles by granular filter media coated with nanoporous aluminium oxide, *Water Sci. Technol.*, 2004, **20**, 223–228.

22 M. Wegmann, B. Michen, T. Luxbacher, J. Fritsch and T. Graule, Modification of ceramic microfilters with colloidal zirconia to promote the adsorption of viruses from water, *Water Res.*, 2008, **429**, 1726–1734.

23 Y. Tang, Z. Liu, K. Zhao and S. Fu, Adsorption and separation properties of positively charged ZrO_2 nanofibrous membranes fabricated by electrospinning, *RSC Adv.*, 2017, **7**, 42505–42512.

24 C. H. Park, C. H. Kim, L. D. Tijing, D. H. Lee, M. H. Yu, H. R. Pant, Y. Kim and C. S. Kim, Preparation and characterization of (polyurethane/nylon-6) nanofiber/(silicone) film composites *via* electrospinning and dip-coating, *Fibers Polym.*, 2012, **13**, 339–345.

25 M. Guo, B. Ding, X. Li, X. Wang, J. Yu and M. Wang, Amphiphobic nanofibrous silica mats with flexible and high-heat-resistant properties, *J. Phys. Chem. C*, 2010, **114**, 916–921.

26 X. Wang, L. Dou, L. Yang, J. Yu and B. Ding, Hierarchical structured $MnO_2@SiO_2$, nanofibrous membranes with superb flexibility and enhanced catalytic performance, *J. Hazard. Mater.*, 2017, **324**, 203–212.

27 Z. Ma, Z. Hu, X. He, Z. Fang, Y. Li and J. Qiu, Nano-Bi_2WO_6 functionalized flexible SiO_2 fibrous film for water purification, *Appl. Surf. Sci.*, 2016, **360**, 174–183.

28 P. C. Wong, Y. S. Li, M. Y. Zhou and K. A. R. Mitchell, XPS investigations of the interactions of hydrogen with thin films of zirconium oxide I. Hydrogen treatments on a 10 Å thick film, *Appl. Surf. Sci.*, 1995, **89**, 255–261.

29 Y. S. Li, P. C. Wong and K. A. R. Mitchell, XPS investigations of the interactions of hydrogen with thin films of zirconium oxide II. Effects of heating a 26 Å thick film after treatment with a hydrogen plasma, *Appl. Surf. Sci.*, 1995, **89**, 263–269.

30 R. Srinivasan, C. R. Hubbard, O. B. Cavin and B. H. Davis, Factors determining the crystal phases of zirconia powers - A new outlook, *Chem. Mater.*, 1993, **5**, 27–31.

31 W. Z. Zhu and M. Yan, Stability of tetragonal phase in ZrO_2 (2 mol% Y_2O_3) ceramics sintered in reducing atmosphere, *J. Mater. Sci. Lett.*, 1997, **16**, 1540–1543.

32 M. Wegmann, B. Michen and T. Graule, Nanostructured surface modification of microporous ceramics for efficient virus filtration, *J. Eur. Ceram. Soc.*, 2008, **28**, 1603–1612.